BPR MCS | Bulletin of Pioneering Researches of Medical and Clinical Science

Bulletin of Pioneering Researches of Medical and Clinical Science

Available online: https://bprmcs.com
2025 | Volume 5 | Issue 1 | Page: 242-259

Synergistic Inhibition of Hepatocellular Carcinoma Growth via Combined mTOR Blockade and Microtubule Disruption

Maria Gonzalez[1]*, Javier Ruiz[1], Lucia Torres[2], Elena Ruiz[1]

[1]Department of Medical Innovation and Clinical Sciences, University of Granada, Granada, Spain.
[2]Department of Translational Medical Systems, University of Seville, Seville, Spain.

Abstract

Hepatocellular carcinoma (HCC) poses considerable therapeutic challenges, given that standard chemotherapies offer only restricted benefit. The mammalian target of rapamycin/sirolimus (mTOR) and microtubules represent two major druggable vulnerabilities in HCC. In this work, we demonstrated that concurrent mTOR inhibition with mTOR inhibitors (everolimus and sirolimus) and the microtubule inhibitor vinorelbine yielded outcomes superior to those of single-agent regimens in HCC PDX models. Our data indicate that vinorelbine halts cells in mitosis, promotes apoptosis, and restores a more normal vascular architecture within tumors, while simultaneously increasing survivin levels and activating the mTOR/p70S6K/4EBP1 signaling axis. Supplementing treatment with everolimus substantially augmented tumor sensitivity to vinorelbine, translating into extended overall survival (OS) across the majority of orthotopic HCC PDX models examined. Mechanistic dissection revealed that this pronounced tumor-suppressive effect correlated with diminished expression of mTOR effectors (p-p70S6K, p-4EBP1, and p-S6K), several pivotal cell-cycle regulatory proteins, and the anti-apoptotic factor survivin. Importantly, these molecular changes did not disrupt the vascular normalization elicited by vinorelbine in vinorelbine-responsive PDX models or by everolimus in everolimus-responsive PDX models. The pairing of everolimus with vinorelbine (everolimus/vinorelbine) also fostered apoptosis while exhibiting minimal toxicity. Given the affordability and documented clinical activity of everolimus and notably sirolimus, this combination strategy warrants further assessment in early-stage clinical trials.

Keywords: Hepatocellular carcinoma, mTOR inhibitor, Microtubule inhibitor, Vessel normalization, Hypoxia

Corresponding author: Maria Gonzalez
E-mail: maria.gonzalez@gmail.com

Received: 12 February 2025
Revised: 23 May 2025
Accepted: 27 May 2025

How to Cite This Article: Gonzalez M, Ruiz J, Torres L, Ruiz E. Synergistic Inhibition of Hepatocellular Carcinoma Growth via Combined mTOR Blockade and Microtubule Disruption. Bull Pioneer Res Med Clin Sci. 2025;5(1):242-59. https://doi.org/10.51847/3W32MQtXb8

Introduction

Hepatocellular carcinoma (HCC) accounts for the second-highest number of cancer-attributable deaths on a global scale [1, 2]. The vast majority of HCCs (> 80%) emerge against a background of liver cirrhosis arising from varied causes such as hepatitis B and C viral infections, heavy alcohol use, diabetes mellitus, and non-alcoholic fatty liver disease (NAFLD) [3]. The inherent intratumor heterogeneity of HCC renders its clinical management particularly complex. For individuals diagnosed with early-stage HCC, surgical excision and liver grafting may offer a curative path [4]—unfortunately, a large proportion of HCC patients present with disease that is not amenable to curative resection. Systemic therapies, including sorafenib and lenvatinib, have conferred survival benefits in patients with advanced-stage HCC [5-7]. While sorafenib [5, 7] and lenvatinib [6] monotherapies provide some benefit, their overall impact remains modest and is frequently undermined by the onset of drug resistance. At

present, combination immunotherapeutic protocols such as atezolizumab plus bevacizumab and durvalumab plus tremelimumab are favored as initial treatment choices, except in individuals exhibiting high-risk indicators for variceal or other gastrointestinal hemorrhage and in cirrhotic patients for whom immune-based treatments are unsuitable (e.g., because of serious autoimmune conditions or liver transplant status) [8, 9]. Investigations exploring lenvatinib combined with anti-PD1 agents in unresectable HCC have also been pursued [10]. Two additional multikinase inhibitors, regorafenib [11] and cabozantinib [12], have received approval in the second-line setting after both demonstrated significantly superior OS relative to placebo in HCC cohorts. Considering the aggressive biology of HCC and its tendency toward early intrahepatic spread [13], the demand for innovative, efficacious, and cost-accessible therapies for this fatal malignancy is acute.

Aberrant signaling through the mammalian target of rapamycin (mTOR) pathway occurs in approximately 45% of HCC cases, and elevated mTOR expression portends a worse clinical outcome [14, 15]. mTOR serves as a central mediator of the PI3K/AKT/mTOR cascade and is critically involved in regulating cell division and survival. Its downstream substrates include the ribosomal p70S6K kinase and the eukaryotic initiation factor eIF4E-binding protein (4E-BP1), both of which orchestrate cell-cycle progression, cellular growth, and protein biosynthesis. Recent evidence has shown that the mTOR inhibitor everolimus selectively blocks DNA synthesis in hepatocytes and profoundly delays the emergence of DNA damage-driven liver neoplasms, underscoring that mTOR pathway activation strongly influences hepatocarcinogenesis [16]. Hence, mTOR constitutes a high-priority molecular target in HCC treatment. A worldwide phase III evaluation of everolimus in HCC patients whose disease had advanced on sorafenib (everolimus for liver cancer evaluation-1 (EVOLVE-1)) did not accomplish its primary goal of demonstrating enhanced OS with everolimus [17]. Given that mTOR inhibition primarily acts in a cytostatic manner [18], deploying mTOR inhibitors as standalone anticancer agents may be inherently limited in value. It is reasonable to hypothesize that combining an mTOR inhibitor with a cytotoxic compound could yield a more potent therapeutic approach than mTOR inhibition alone.

Microtubule-governed cellular architecture and organization are fundamental to HCC pathogenesis [19-21], modulating not only mitotic division but also cytoskeletal integrity, cell locomotion, and the trafficking of intracellular proteins and organelles [22]. As a result, agents that disrupt microtubule function inhibit cell proliferation by inducing cell-cycle arrest and programmed cell death, making them potentially valuable therapeutic targets in HCC [21]. Within this class of agents, vinorelbine has shown radiosensitizing properties even at low concentrations [23, 24]. In clinical studies demonstrating its safety and antitumor efficacy, vinorelbine has been used as a standard backbone in concurrent chemoradiotherapy protocols for patients with lung cancer [25, 26]. Our earlier work has shown that vinorelbine, when co-administered with the FGFR1-3 inhibitor infigratinib [27], the FGFR4 inhibitor FGF401 [28], or ionizing radiation [29], effectively suppresses HCC tumor growth in vivo.

Both the microtubule network and the mTOR pathway are tractable pharmacological targets, and compounds directed against them have already reached the clinic and are widely accessible for other disease indications. In the current investigation, we set out to characterize the tumor-inhibitory capacity of vinorelbine when combined with mTOR inhibitors (everolimus and sirolimus) and to decipher the mechanisms underlying the suppression of HCC tumor expansion by this combination. Our initial objective was to determine whether the addition of everolimus enhanced the antitumor activity of vinorelbine. Next, we examined whether vinorelbine modifies tumor vascularization, tumor hypoxia, and overall survival in animals with orthotopic HCC tumors. Lastly, we sought to clarify whether the retardation of tumor progression stemmed from decreased neoplastic cell proliferation, heightened tumor cell death, or both. We describe here the impact of vinorelbine monotherapy and in combination with either everolimus or sirolimus across patient-derived xenograft (PDX) models of human HCC.

Materials and Methods

The reagents, isolation and cultivation of HCC cells, vessel perfusion experiments, tumor harvest and tissue processing, immunohistochemistry (IHC), slide scanning and quantitation, western blotting, orthotopic model establishment, and statistical computations were executed or set up as detailed in prior publications [27, 30-32].

Reagents

Vinorelbine (Navelbine®) (10 mg/mL) was procured from Pierre Fabre Medicament (Boulogne, France) and was diluted in PBS to reach a final working concentration of 0.375 mg/mL. Everolimus (RAD001) was obtained from Novartis (Basel, Switzerland) and was reconstituted in vehicle (30% Captisol® in water) to yield the appropriate strength for dosing.

Antibodies recognizing AKT (#9272), p70S6K (#9202), survivin (#2803), S6R (#2217), Rb (#9313), Cyclin B1 (#4138), eIF4E (#9742), Cdc25C (#4688), cleaved caspase 3 (#9661), cleaved caspase 7 (#9491), cleaved PARP (#5625), Cyclin D1 (#2978), Cdc2 (#9112), and α-Tubulin (#2144), along with phospho-specific antibodies directed against RB Ser807/811 (#9308), AKT Ser473

(#9271), mTOR Ser2448 (#5536), p70S6K Thr421/424 (#9204), S6R Ser235/236 (#4858), 4EBP1 Thr70 (#9455), Histone H3 Ser10 (#9701), Cyclin D1 Thr286 (#3300), Cdc25C Ser216 (#4901), Cdc2 Tyr15 (#9111), eIF4E Ser209 (#9741), and ERK1/2 Thr202/Tyr204 (#4370), were sourced from Cell Signaling Technology (Beverly, MA, USA). RKIP (#37-2100) was acquired from Invitrogen. p-Cdk2 Thr14/Tyr15 (sc-28435-R), ERK1/2 (sc-94), and p27 (sc-528) were purchased from Santa Cruz Biotechnology Inc. (Santa Cruz, CA, USA). Anti-mouse CD31 (#2502) antibody was obtained from BioLegend (San Diego, CA, USA).

Patient-Derived Xenograft (PDX) HCC models

Ethical oversight for this study was provided by the SingHealth Centralised Institutional Review Board, which approved the study (ethics code: CIRB #2006/435/B; approval date: 2 October 2018). Husbandry and experimental use of all rodents conformed to the stipulations detailed within the Guide for the Care and Use of Laboratory Animals, as disseminated by the National Institutes of Health, USA [33].

Establishment of xenograft lines from HCC tumors had been performed previously [31]. A collection of 15 such HCC xenograft lines (HCC01–0708, HCC05–0411B, HCC05–0614, HCC06–1009, HCC09–0913, HCC13–0109, HCC13–0212, HCC19–0509, HCC19–0913, HCC24–0309, HCC25–0705A, HCC26–0808B, HCC27–1014, HCC29–0909A, and HCC30–0805B) was selected for tumor propagation in male SCID mice (InVivos, Singapore) whose ages fell between 9 and 10 weeks. Working under sterile conditions, the HCC xenograft material was diced into tiny fragments sufficiently small to be drawn through an 18-gauge needle, after which it was mixed with Matrigel® (Corning Inc., Corning, NY, USA) at a 1:1 (v/v) proportion to produce a uniform suspension totaling 150 µL for each inoculation. This admixture was then introduced subcutaneously into both flanks of every mouse. Lesion development was followed at least biweekly until the tumor volumes fell within the 170–200 mm^3 range.

The animals were maintained in negative-pressure isolator cabins at 23 °C and 43% relative humidity, on a 12 h light/12 h dark rhythm, with unlimited access to sterilized feed and drinking water. All procedures were conducted in full compliance with protocols ratified by the IACUC.

Drug treatment and efficacy of everolimus/vinorelbine in ectopic PDX HCC models

To delineate how vinorelbine influences apoptosis, cell division, intratumoral vessel density, and vascular normalization over a time course, mice bearing HCC13–0212 tumors received intraperitoneal dosing of either the vehicle (PBS) or vinorelbine at a concentration of 3 mg/kg. Administration was begun once tumor sizes had entered the range of approximately 250–300 mm^3. Neoplastic tissues were excised at 0, 24, 36, 48, 60, and 72 h after treatment and then submitted for IHC processing.

For the dual-therapy evaluation, animals implanted with the aforementioned HCC xenograft lines were sorted at random into four arms (n = 8–10) that followed the subsequent dosing scheme: (a) vehicle co-delivered with PBS, (b) 2 mg/kg of everolimus (standard dose) co-delivered with PBS, (c) 3 mg/kg of vinorelbine co-delivered with vehicle, or (d) 2 mg/kg of everolimus co-delivered with 3 mg/kg of vinorelbine (everolimus/vinorelbine) over the indicated timeframe. The regimen included a once-daily oral gavage schedule for both vehicle and everolimus. At the same time, PBS and vinorelbine were injected into the peritoneal cavity at 2 doses per week (separated by 3.5 days). In all cases, therapy commenced after the tumors achieved roughly 170–200 mm^3. Tumor dimensions, body mass, and any outward signs of compromised health were carefully observed and annotated in accordance with the procedures outlined in earlier reports [27-29, 34]. When each experiment reached its predefined endpoint, the mice were euthanized, and the tumors were dissected out, weighed, and cataloged. The surgically removed tumors were partitioned: one segment was rapidly cryopreserved in liquid nitrogen for subsequent molecular workup, and the remaining segment was placed into 10% formalin and taken forward for IHC analysis. The entire set of experiments was rerun using the chosen HCC xenografts, substituting sirolimus for everolimus.

Activity of the everolimus, vinorelbine, and everolimus/vinorelbine conditions across the HCC PDX set was gauged by computing the T/C metric, which reflects the quotient of the median tumor mass in the drug-receiving group (T) over that in the vehicle-receiving group (C) upon treatment completion. T/C values below 0.42 were scored as active, consistent with the classification system of the Cancer Therapy Evaluation Program (CTEP) of the Investigational Drug Branch (IDB) at the National Cancer Institute [34].

Vessel perfusion and hypoxia studies

Examinations of vascular perfusion and oxygen deficit were performed as described earlier in Huynh *et al*. [27]. Mice harboring neoplastic growths (given either vehicle or test compounds) were infused intravenously with 100 mg of biotin-conjugated tomato lectin (isolated from *Lycopersicon esculentum*) (Vector Labs, Newark, CA, USA, #B-1175) suspended in 100 µL of 0.9% NaCl, after which they were dosed intraperitoneally with 60 mg/kg pimonidazole hydrochloride. The tumors were removed 2 h following lectin delivery and hypoxia marker injection, placed into 10% formalin, and processed for the assays that followed. To highlight functional microvessels, tissue sections were subjected to IHC staining employing the

streptavidin–biotin peroxidase complex technique as specified by the kit manufacturer (Lab Vision Corporation, Fremont, CA, USA). To evaluate the extent of hypoxia, oxygen-deprived zones within tumors were visualized by applying the Hypoxyprobe Plus Kit HP2 to sections according to the supplier's instructions (Hypoxyprobe Inc., Burlington, MA, USA). For the numerical analysis, ten non-overlapping 0.159 mm^2 areas were randomly selected, imaged at 100× magnification, and manually counted on every IHC-processed slide.

Immunohistochemistry (IHC)

IHC staining was performed as described in a previous report [32]. Sections were incubated with primary antibodies targeting CD31 (Cell Signaling Technology, #77699); phosphorylated histone H3 at serine 10 (Cell Signaling Technology, #9701); and cleaved PARP (Cell Signaling Technology, #5625) to gauge, respectively, the density of microvessels, the extent of mitotic activity, and the level of programmed cell death. No fewer than ten distinct microscopic fields were arbitrarily selected and photographed at a 100× magnification setting on an Olympus BX60 system (Olympus, Tokyo, Japan) for every IHC-processed slide. Quantitative determination of mean microvessel density, together with proportions of p-histone H3 Ser10- and cleaved PARP-immunoreactive cells, was accomplished by tallying all positively marked cells within the digitized images and normalizing these counts as a percentage of the overall cellularity in the corresponding field.

Cell cultures

Single-cell suspensions were prepared from HCC13–0109 and HCC25–0705A tumor masses and established as two-dimensional monolayer cultures in high-glucose Dulbecco's modified Eagle medium (DMEM) containing 10% fetal bovine serum (FBS) along with 1% penicillin–streptomycin, kept at 37 °C in a humidified incubator with 5% CO_2, as previously documented [32].

Propidium iodide (PI) flow cytometry analysis

HCC13–0109 and HCC25–0705A lines were readied according to an earlier published procedure [32]. Cells were distributed into plates at 5×10^5 per well and subsequently challenged with vehicle alone, 0.1 μM everolimus, or 1 nM vinorelbine diluted in culture medium for 24 h. Fixation was achieved by immersing the cells in 70% ethanol and holding them at 4 °C for 24 h. Following this step, the cells underwent rehydration, a PBS wash, digestion with ribonuclease A (RNase A; 1 mg/mL), and labeling with propidium iodide (PI) at 100 μg/mL. Fluorescent signals from the stained populations were recorded on a FACSCalibur™ flow cytometer (BD, San Jose, CA, USA). The resulting datasets were processed using BD CellQuest™ Pro software (Version 4.1; BD, San Jose, CA, USA), as outlined in a prior publication [27]. A total of 10,000 events were gathered per reading, with gating parameters set to discriminate against doublet aggregates. The distribution of DNA within specific cell-cycle compartments is depicted as a percentage of the total gated DNA. Values shown correspond to the mean derived from three independent biological replicates.

Serum analysis

Serum was harvested from mice subjected to 14 consecutive days of treatment with vehicle, everolimus, vinorelbine, or the everolimus/vinorelbine combination. The collected sera were assayed for a panel of biomarkers—total bilirubin (TBIL), alkaline phosphatase (ALP), alanine aminotransferase (ALT), aspartate aminotransferase (AST), albumin (ALB), creatinine (Cre), glucose (GLU), and blood urea nitrogen (BUN)—by means of the preventive care profile plus analyzer (Abaxis Inc., Union City, CA, USA) following the vendor's protocol.

Western blot analysis

To examine modulations in protein abundance between tumors from vehicle-dosed and drug-dosed cohorts, snap-frozen specimens were mechanically disrupted in a homogenization buffer formulated with 50 mM Tris-HCl (pH = 7.4), 150 mM NaCl, 0.5% NP-40, 1 mM EDTA, and 25 mM NaF, further fortified with protease inhibitor cocktail and 10 mM Na_3VO_4. An aliquot containing 80 μg of total protein from each lysate was separated on an SDS–PAGE gel and subsequently transferred to a nitrocellulose membrane, as described in Huynh *et al*. [27]. The membranes were sequentially probed with the designated primary antibodies and appropriate horseradish peroxidase-coupled secondary antibodies. Immunoreactive bands were visualized using a chemiluminescent substrate kit (Amersham Pharmacia Biotech, Amersham, UK) and recorded on X-ray film.

Efficacies of everolimus, vinorelbine, and everolimus/vinorelbine in orthotopic PDX HCC models

Orthotopic tumor models utilizing HCC13–0212, HCC24–0309, and HCC25–0705A were constructed as detailed elsewhere [30]. In brief, SCID mice were rendered unconscious with an intramuscular dose of a ketamine/diazepam admixture (50 mg/kg ketamine hydrochloride; Rotexmedica, Trittau, Germany; plus 5 mg/kg diazepam (Atlantic)). An intramuscular injection of Baytril® at 5 mg/kg was concurrently delivered. Working within a sterile field, a short upper midline laparotomy incision was made to bring the left hepatic lobe into view gently. A quantity of roughly 5×10^6 neoplastic cells, suspended in 30 μL of a culture medium–Matrigel slurry, was introduced into the liver parenchyma via a 27-gauge

needle. Closure of the incision was accomplished with a running 5-0 silk suture. For the survival arm of the study, mice harboring orthotopic HCC lesions (n = 10 per treatment condition) were assigned to receive vehicle, everolimus, vinorelbine, or everolimus/vinorelbine according to the dosing parameters outlined above. Therapy commenced once the estimated tumor volume fell within the 100–150 mm^3 range. Body mass and overall survival were recorded every day. Animals were removed from the study and euthanized upon reaching a moribund condition.

Statistical analysis

Differences among groups with respect to tumor volumes, excised tumor weights, terminal body weights, and mean counts of p-histone H3 Ser10-positive, cleaved PARP-positive, CD31-positive, and lectin-perfused cells were subjected to formal comparison. Pairwise evaluations between two groups were conducted using Student's t-test. When the analysis involved three or more groups, one-way analysis of variance (ANOVA) was used, supplemented by the Tukey–Kramer post hoc adjustment. Error bars throughout represent the computed standard deviation (SD) values. Survival curve comparisons relied on the log-rank test. A probability value of < 0.05 was taken to indicate statistical significance.

Results and Discussion

Vinorelbine displayed antimitotic and apoptosis-inducing actions, attenuated tumor hypoxia via vascular normalization, and raised the levels of mTOR pathway downstream components (p-p70S6K/4EBP1/Survivin) in HCC PDX models

Our initial experiments assessed the tumor-suppressive effects of vinorelbine at 3 mg/kg, dosed twice weekly. Compared against the vehicle-treated reference group, vinorelbine brought about a considerable deceleration of tumor progression kinetics in the HCC13–0109, HCC25–0705A, HCC13–0212, HCC19–0913, HCC05–0614, HCC19–0509, HCC26–0808B, and HCC24–0309 PDX lines, as illustrated in **Figure 1**. By contrast, only a muted response was registered in the HCC29–0909A, HCC27–1014, HCC01–0708, HCC09–0913, and HCC06–1009 PDX lines. Across all models, barring the HCC05–0411B line, the neoplastic masses harvested from vinorelbine-dosed animals weighed significantly less than those collected from the vehicle-dosed cohort **(Figure 1)**. Of the 15 HCC PDX models challenged with vinorelbine, five (33.3%, namely HCC13–0109, HCC13–0212, HCC19–0509, HCC19–0913, and HCC25–0705A) attained T/C ratios below the 0.42 cutoff **(Table 1)**.

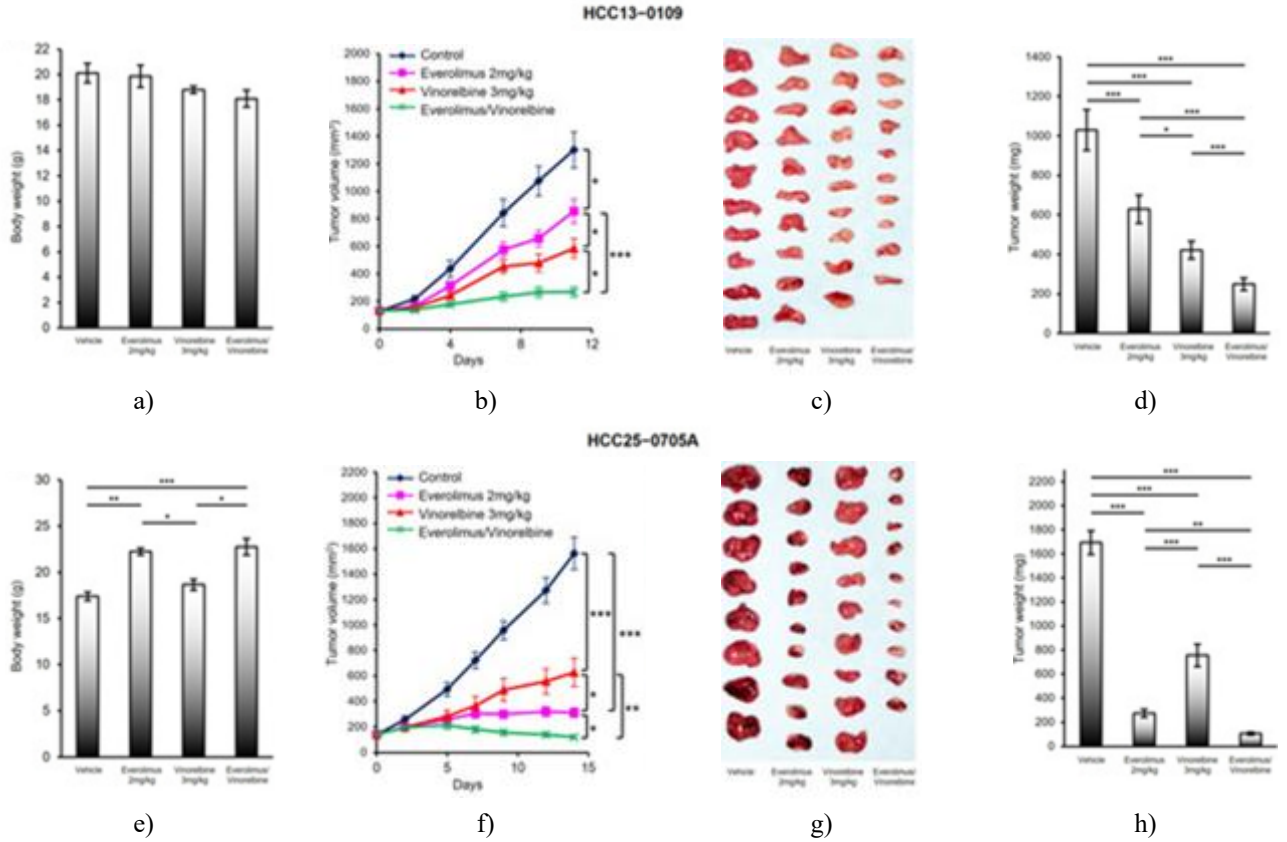

Figure 1. Consequences of everolimus, vinorelbine, and the everolimus/vinorelbine dual regimen on tumor progression within the HCC13–0109 and HCC25–0705A PDX models. Specimens of HCC tumors were inoculated subcutaneously into SCID mice according to the protocols outlined in Section 4. Rodents carrying the designated neoplasms were randomly allocated across four groups and dosed via oral gavage with 200 µL of vehicle solution, everolimus alone at 2 mg/kg once per day, vinorelbine alone at 3 mg/kg spaced 3.5 days apart, or concurrent everolimus (2 mg/kg) plus vinorelbine (3 mg/kg)

on the indicated days. Each treatment condition comprised between 8 and 10 independently tumor-bearing animals. Shown here are (a, e) the average body masses ± SE registered at the time of sacrifice; (b, f) the average tumor dimensions ± SE captured at successive time intervals; (c, g) representative macroscopic images of tumor specimens collected from the vehicle-, everolimus-, vinorelbine-, and everolimus/vinorelbine-exposed cohorts; and (d, h) the average matched tumor masses ± SE. Varied asterisk notation identifies statistically meaningful divergences ($P < 0.05$; $P < 0.01$; $P < 0.001$; one-way ANOVA supplemented by Tukey's comparison).

Table 1. Impact of everolimus (or sirolimus), vinorelbine, and the everolimus (or sirolimus)/vinorelbine combination on neoplastic burden assessed across the HCC PDX collection. The specified tumor lines were propagated as subcutaneous xenografts in SCID mice exactly as detailed in Section 4. Tumor-bearing animals were sorted at random into four cohorts and dosed orally with 200 µL of vehicle preparation, everolimus (or sirolimus) monotherapy at 2 mg/kg delivered once per day, vinorelbine monotherapy at 3 mg/kg injected twice weekly (every 3.5 days), or a joint regimen of everolimus (or sirolimus) at 2 mg/kg plus vinorelbine at 3 mg/kg for the designated duration. Every treatment condition contained 8–10 individually engrafted mice. Mean tumor mass was registered, and the potency of each intervention was quantified using the T/C formula, where T signifies the median tumor mass in the drug-receiving cohort and C the median tumor mass in the corresponding vehicle-receiving cohort at the point of treatment cessation. The resulting T/C ratios are presented.

HCC PDX Model ID	Control (T/C)	Sirolimus + Vinorelbine	Sirolimus (2 mg/kg, QD)	Everolimus + Vinorelbine	Vinorelbine (3 mg/kg, Q3.5D)	Everolimus (2 mg/kg, QD)
HCC05–0411B	1	–	–	0.1389	0.6707	0.1883
HCC06–1009	1	0.1919	0.3958	0.2031	0.5650	0.2931
HCC24–0309	1	–	–	0.0698	0.5142	0.1218
HCC26–0808B	1	–	–	0.1780	0.5775	0.1886
HCC13–0212	1	0.1292	0.3785	0.0656	0.1966	0.3359
HCC19–0509	1	–	–	0.2319	0.3348	0.3754
HCC25–0705A	1	–	–	0.0635	0.3869	0.1622
HCC01–0708	1	–	–	0.3345	0.7542	0.5767
HCC05–0614	1	–	–	0.1523	0.5105	0.5395
HCC09–0913	1	–	–	0.3314	0.6651	0.5645
HCC13–0109	1	–	–	0.2419	0.3092	0.6108
HCC19–0913	1	0.1691	0.5888	0.1669	0.3192	0.5770
HCC27–1014	1	–	–	0.3332	0.5866	0.7707
HCC29–0909A	1	–	–	0.3680	0.5671	0.6287
HCC30–0805B	1	0.2041	0.6176	–	0.6080	–

When measured against the vehicle-receiving group, vinorelbine elicited substantial alterations in the HCC19–0913, HCC13–0109, HCC25–0705A, HCC13–0212, and HCC24–0309 PDX lines, reflected by a rise in the frequency of p-histone H3 Ser10-immunoreactive nuclei, an expansion of the intratumoral vascular network, and an accumulation of cleaved PARP-immunopositive cells. The tumor vasculature in vehicle-dosed specimens was characterized by grossly aberrant architecture, with vessels adopting contorted, irregular configurations typical of pathological vascular remodeling. In sharp contrast, the vinorelbine-exposed tumors were replete with fine, capillary-like conduits, a phenotype captured in **Figure 2**. In contrast, the HCC29–0909A, HCC09–0913, HCC30–0805B, and HCC29–1104 PDX lines challenged with vinorelbine developed only negligible increments in either apoptotic or mitotic cell populations. Consistent with this weak pharmacodynamic response, each of these models yielded T/C ratios above the 0.42 benchmark, as shown in **Table 1**, indicating their innate resistance to vinorelbine. Tellingly, vinorelbine did not appreciably convert the vascular phenotype toward the slender, normalized appearance in any of the four resistant models—HCC29–0909A, HCC09–0913, HCC30–0805B, or HCC29–1104. These data suggest strong concordance between vinorelbine's vascular remodeling activity and its overall antitumor potency. Parallel trends were noted when evaluating other HCC PDX models from the panel under vehicle or vinorelbine conditions.

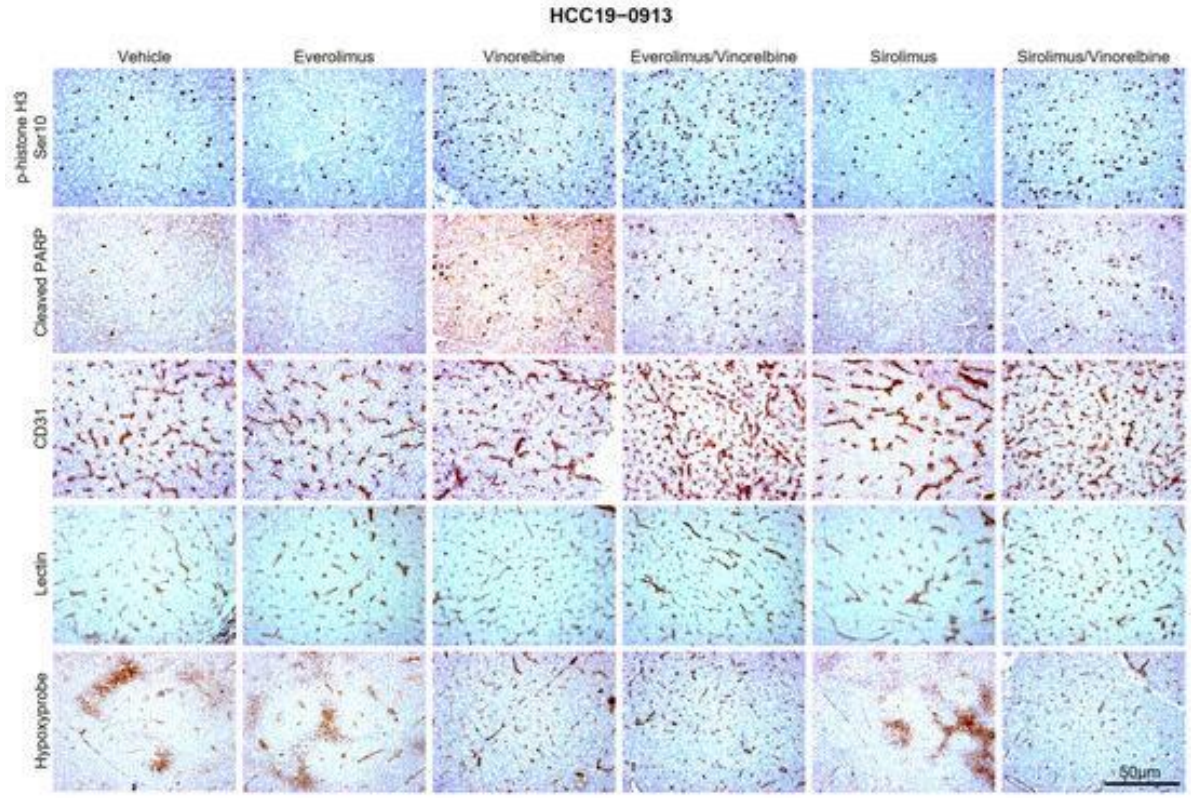

Figure 2. Pharmacodynamic effects of everolimus (or sirolimus), vinorelbine, and everolimus (or sirolimus)/vinorelbine on tumor cell division, apoptotic death, vascular density, vessel normalization, and regional oxygen deficiency. HCC19–0913 tumor tissue was inoculated subcutaneously into SCID mice, as described in Section 4. Animals bearing the designated tumors were allocated at random to one of four dosing regimens and received, by oral gavage, 200 μL of either vehicle solution, everolimus (or sirolimus) at 2 mg/kg given daily, vinorelbine at 3 mg/kg given twice weekly (every 3.5 days), or the pairing of everolimus (or sirolimus) at 2 mg/kg plus vinorelbine at 3 mg/kg for the specified number of days. Each group was composed of 8–10 independently tumor-bearing mice. Tumors were harvested at 2-hour intervals following the last administered dose and subsequently processed for IHC as detailed in Section 4. Shown are representative stained cross-sections from vehicle- and drug-treated animals, visualized with antibodies detecting p-histone H3 Ser10 (mitotic marker), cleaved PARP (apoptotic marker), CD31 (pan-endothelial labeling of blood vessels), lectin (functionally perfused vasculature), and Hypoxyprobe (areas of low oxygen tension). Photomicrographs were taken using an Olympus BX60 microscope (Olympus, Tokyo, Japan). Scale bars denote 50 μM.

In the HCC13–0212 model, which proved sensitive to vinorelbine, dosing tumor-bearing mice with 3 mg/kg of vinorelbine triggered a pronounced elevation in the proportion of cells immunoreactive for p-histone H3 Ser10 within the first 24 hours. This fraction reached its zenith by the 48-hour mark and subsided to near-baseline values at 72 hours following drug administration. Concurrently, meaningful programmed cell death—revealed by the enumeration of cleaved PARP-stained cells—was evident as early as 24 hours and escalated progressively to attain maximal levels at the 72-hour time point post-vinorelbine delivery. Alongside these changes, the density of microvessels rose considerably and likewise peaked at 72 hours.

To gauge the operational status of the amplified vascular network in vinorelbine-dosed tumors, biotin-tagged tomato lectin (from *Lycopersicon esculentum*) was delivered intravenously to both vehicle-treated and vinorelbine-treated mice. This step enabled fluorescent tagging of the murine endothelial compartment and permitted discrimination between anatomically present vessels and those actively conveying blood flow. Pimonidazole HCl was then administered systemically to map oxygen-depleted microdomains within the neoplastic mass. As illustrated in **Figure 2**, lectin adherence to the endothelium was strikingly limited in vehicle-treated tumors belonging to the HCC19–0913, HCC13–0109, HCC25–0705A, HCC13–0212, and HCC24–0309 PDX panels. Large swaths of tissue were entirely unstained by lectin, consistent with the interpretation that a predominant fraction of vessels in these untreated neoplasms were functionally inert. Regions with strong Hypoxyprobe reactivity occupied much of the tumor's cross-sectional area, corroborating widespread oxygen scarcity. In diametric opposition, the slender, capillary-like vessels engendered by vinorelbine exposure were amply decorated with biotinylated lectin, confirming that the majority were well perfused. Moreover, Hypoxyprobe

reactivity was largely extinguished across extensive portions of the tumors, reflecting restored tissue oxygenation and underscoring that vinorelbine re-established physiological oxygen delivery. When considered together, the perfusion and hypoxia assessments strongly support the conclusion that vinorelbine promotes the functional normalization of the tumor circulatory network.

Western blot profiling demonstrated that a 3-day vinorelbine regimen led to conspicuous upregulation of both p-p70S6K (at Thr389 and Thr421/424) and p-4EBP1 (Thr70) within vinorelbine-sensitive HCC19–0913 tumors, indicative of heightened signaling through the mTOR effector axis.

We subsequently shifted focus to delineate the antineoplastic properties of everolimus as a standalone intervention. As summarized in **Figure 1, Table 1**, once-daily oral delivery of everolimus (or sirolimus) at 2 mg/kg produced a robust suppression of tumor outgrowth in the HCC24–0309, HCC25–0705A, HCC05–0411B, HCC19–0509, and HCC26–0808B PDX lines, designating these as relatively susceptible to mTOR-directed therapy. Within these responding models, the final tumor dimensions recorded in the everolimus-treated cohorts were approximately 3- to 8-fold smaller than those observed in the vehicle-exposed cohorts. In striking contrast, tumor volumes in the everolimus-dosed HCC01–0708, HCC05–0614, HCC09–0913, HCC13–0109, HCC19–0913, HCC27–1014, and HCC29–0909A PDX lines either failed to shrink significantly or exhibited only trivial decrements relative to vehicle-dosed controls, classifying these as intrinsically less responsive to mTOR inhibition. Applying the T/C < 0.42 efficacy criterion, everolimus qualified as active in 7 of the 14 (50%) HCC PDX models screened (specifically, HCC05–0411B, HCC06–1009, HCC13–0212, HCC19–0509, HCC24–0309, HCC25–0705A, and HCC26–0808B). mTOR blockade also yielded significant expansions of both total vessel numbers and functionally perfused vessel counts, accompanied by attenuation of tumor hypoxia, within the mTOR-responsive HCC25–0705A and HCC24–0309 PDX models. This vascular remodeling signature did not extend to the vinorelbine-responsive HCC19–0913, HCC13–0109, and HCC13–0212 PDX models **(Figure 2)**. Instead, everolimus-treated HCC13–0109 and HCC13–0212 tumors contained fewer total vessels and fewer perfused vessels than their vehicle-treated counterparts, implying that everolimus exhibits an anti-angiogenic mode of action within these specific tumor contexts.

The antitumor synergy achieved by everolimus (or sirolimus) added to vinorelbine

Our demonstration that vinorelbine both normalized the vascular network **(Figure 2)** and paradoxically reinstated mTOR-dependent signaling outputs laid the groundwork for the next logical step: evaluating whether the concurrent engagement of mTOR with everolimus or sirolimus, alongside microtubule disruption with vinorelbine, would deliver superior anticancer efficacy in the HCC PDX collection—a panel deliberately chosen to capture a spectrum of drug sensitivities. The conceptual framework underlying this dual approach was twofold: the vessel-normalizing action contributed by either agent class was anticipated to enhance intratumoral drug penetration, thereby yielding both greater tumor shrinkage and a meaningful extension of host survival.

Accordingly, the entire 15-member HCC PDX panel was enrolled into a randomized four-arm design comprising (a) vehicle, (b) vinorelbine only, (c) everolimus only, and (d) everolimus paired with vinorelbine, following the procedures outlined in Section 4. The resultant sensitivity classification distributed the 15 tested lines as follows: four were preferentially mTOR-inhibitor-responsive, two showed selective vinorelbine responsiveness, three displayed dual sensitivity, and the remaining six were refractory to both single modalities **(Table 1)**.

Excluding HCC26–0808B, whose exquisite everolimus responsiveness precluded any meaningful scope for further augmentation, all 14 of the remaining HCC PDX models experienced a substantially larger degree of tumor growth attenuation and a more profound diminution of ultimate tumor load under everolimus/vinorelbine compared with either drug administered individually **(Figure 1)**. Analogous trends were recapitulated when sirolimus replaced everolimus in the HCC06–1009, HCC13–0212, HCC19–0913, and HCC30–0805B lines **(Table 1)**. Perhaps most compellingly, every single one of the 14 combination-treated HCC PDX models (100%)—a cohort that notably encompassed five lines previously categorized as dual-resistant to everolimus and vinorelbine monotherapy (HCC01–0708, HCC05–0614, HCC09–0913, HCC27–1014, and HCC29–0909A)—registered T/C ratios of < 0.37, thereby decisively clearing the T/C < 0.42 activity threshold set by the Cancer Therapy Evaluation Program (CTEP) of the Investigational Drug Branch (IDB, Bethesda, MD, USA) at the National Cancer Institute **(Table 1)** [34]. Such universal activity underscores that the integration of mTOR inhibition powerfully sensitized tumors to vinorelbine. Concerning tolerability, no appreciable body mass reduction ($P = 0.6543$) nor any manifest clinical indicators of treatment-related morbidity distinguished the treated mice from their vehicle-dosed counterparts.

To reinforce tolerability assessment through objective measures, we performed a comprehensive serum-based liver function panel on blood specimens collected from HCC PDX tumor-bearing mice following exposure to vehicle, everolimus, vinorelbine, or

everolimus/vinorelbine. Daily everolimus dosing was associated with slight upward shifts in ALT, ALP, AST, and TBIL, as tallied in **Table 2**. This observation echoes the well-documented clinical safety record of everolimus [17, 35, 36], in which elevated hepatic enzymes are detected in approximately one-quarter of recipients; however, the elevations are typically of low magnitude and rarely prompt either dose adjustment or permanent cessation of therapy. Vinorelbine, when compared directly against everolimus, provoked somewhat larger increases in the same four hepatic biomarkers, suggesting a mild perturbation of hepatocellular function. Notably, vinorelbine—but not everolimus—also produced a 1.2-fold rise in BUN. In the clinical treatment landscape, vinorelbine administration is associated with elevations in transaminase levels in approximately 5%–10% of patients [37]. Despite its mechanistic cytotoxicity toward dividing cancer cells coupled with robust hepatic clearance, clinically meaningful liver injury attributable to vinorelbine has remained an uncommon occurrence [37]. Whenever Olimus was co-administered with vinorelbine, there were further mild numerical increases in BUN, ALT, ALP, AST, and TBIL relative to vinorelbine alone. However, none of these additional increments reached statistical significance **(Table 2)**. Serum GLU and ALB remained essentially static and showed no meaningful divergence across the four experimental conditions relative to the vehicle-injected group. Synthesizing these data, the combination of everolimus/vinorelbine, like vinorelbine monotherapy, was associated with a profile consistent with mild hepatic stress.

Table 2. Serum biochemical changes associated with everolimus, vinorelbine, and everolimus/vinorelbine exposure with respect to markers of hepatic and renal status. Terminal blood draws were performed on HCC13–0109 tumor-bearing mice that had undergone a 14-day course of treatment with vehicle, everolimus alone, vinorelbine alone, or the everolimus/vinorelbine dual regimen. The harvested serum specimens were processed through the preventive care profile plus analytical system (Abaxis Inc., Union City, CA, USA) strictly per the vendor's recommended workflow. Hepatic integrity was gauged by quantifying total bilirubin (TBIL), alkaline phosphatase (ALP), alanine aminotransferase (ALT), aspartate aminotransferase (AST), and albumin (ALB) in the circulation. Renal function was assessed by measuring serum creatinine (Cre), glucose (GLU), and blood urea nitrogen (BUN).

Serum marker	Unit	Everolimus/ Vinorelbine	Vinorelbine 3 mg/kg Q3.5D	Everolimus 2 mg/kg QD	Control
BUN	(mg/dL)	16.8	16.5	13.1	13.8
CRE	(mg/dL)	0.46	0.49	0.38	0.45
ALT	(U/L)	62.8	69.5	54.5	38.7
ALP	(U/L)	89.2	88.2	73.7	54.1
AST	(U/L)	308.5	279.0	254.6	195
TBIL	(mg/dL)	0.39	0.38	0.32	0.3
GLU	(mg/dL)	188	156.9	170.4	163.2
ALB	(g/dL)	3.6	3.7	3.75	4.0

Following this, we evaluated how each treatment modality influenced the intratumoral vasculature, vessel functionality, oxygen deprivation status, mitotic index, and programmed cell death. Relative to tumors harvested from animals receiving either vehicle or everolimus alone, those exposed to vinorelbine or everolimus/vinorelbine—most prominently within the HCC19–0913, HCC13–0109, and HCC13–0212 PDX lines—demonstrated a two- to five-fold enrichment in the fraction of cells bearing positive staining for p-histone H3 Ser10 **(Figure 2)**. Nonetheless, when the comparator was shifted to vinorelbine monotherapy, the superimposition of everolimus produced divergent outcomes: it either left the proportion of p-histone H3 Ser10-immunoreactive cells largely unperturbed (as seen in HCC19–0913, HCC13–0212, and HCC13–0109) **(Figure 2)** or elicited a marked contraction of this population (as observed in HCC25–0705A).

Across the vinorelbine-responsive HCC PDX lines (HCC19–0913 and HCC13–0109), the model exhibiting dual sensitivity to vinorelbine and mTOR blockade (HCC13–0212), and the mTOR-responsive line (HCC24–0309), the everolimus/vinorelbine combination yielded a 1.5- to 10-fold boost in cleaved PARP-positive cell percentages, coupled with significantly elevated total microvessel counts (ranging from 1.5- to 2.5-fold) when set against either single-agent arm **(Figure 2)**. Moreover, lectin perfusion assays combined with Hypoxyprobe immunolabeling confirmed that the slender, capillary-like vascular structures populating these tumors were adequately perfused and operationally competent, thereby substantially alleviating intratumoral oxygen deprivation. It is worth underscoring, however, that

everolimus/vinorelbine did not appreciably alter the degree of vascular normalization or hypoxia relief beyond what was already elicited by vinorelbine in vinorelbine-responsive PDX models or by everolimus in everolimus-responsive PDX models **(Figure 2)**.

In the HCC25–0705A line, which was responsive to both mTOR inhibition and vinorelbine, the addition of everolimus to vinorelbine did not further augment cleaved PARP immunoreactivity above the levels attained with either vinorelbine or everolimus monotherapy. Likewise, within the HCC PDX models categorized as dual-resistant to both vinorelbine and mTOR inhibitors (HCC29–0909A, HCC09–0913, HCC30–0805B, and HCC29–1104), everolimus/vinorelbine failed to induce meaningful shifts in the abundance of p-histone H3 Ser10-positive cells, cleaved PARP-positive cells, or total vessel density relative to vehicle, everolimus-alone, or vinorelbine-alone conditions. Taken as a whole, these findings indicate that pairing vinorelbine with mTOR inhibitors curbed neoplastic expansion principally by heightening apoptotic cell death, bolstering vascular perfusion, and diminishing tumor hypoxia. To corroborate these mechanistic insights, we performed propidium iodide (PI) flow cytometry to quantify the proportion of cells undergoing apoptosis and the fraction arrested in mitosis at 24 h post-treatment. As tabulated in **Table 3**, everolimus administration was associated with a significant accumulation of cells in the G1 compartment and a concomitant drop in the G2/M population. Conversely, vinorelbine expanded the G2/M pool while shrinking the G1 fraction. The combined treatment further elevated the G2/M percentage beyond that achieved with vinorelbine alone. In addition, both vinorelbine and the everolimus/vinorelbine combination led to a significant increase in the sub-G1 cell population, consistent with the observed increase in apoptosis.

Table 3. Assessment of cell-cycle phase distribution in HCC13–0109 and HCC25–0705A tumor cells. Disaggregated single cells obtained from HCC13–0109 and HCC25–0705A neoplastic tissues were dispensed into culture vessels at a seeding number of 5×10^5 and were then challenged for 24 hours with either vehicle alone, everolimus at a concentration of 0.1 μM, or vinorelbine at a concentration of 1 nM prepared in growth-supporting medium. Upon completion of the incubation, the cellular material was immersed in 70% ethanol for a 24-hour fixation step, subsequently rehydrated, rinsed thoroughly in phosphate-buffered saline, enzymatically digested with ribonuclease A, and ultimately counterstained with PI. The methodology for resolving the DNA histogram into cell-cycle compartments followed the protocol previously detailed in Huynh *et al*. [27]. The relative DNA allotment attributable to each phase is expressed as a percentage of the entire gated DNA population. Reported values correspond to the arithmetic mean derived from three independent biological repetitions.

HCC cell line	Treatment regimen	G2/M phase (%)	S phase (%)	G1 phase (%)	Sub-G1 phase (%)
HCC13–0109	Vehicle (control)	30.94 ± 2.10	3.80 ± 0.42	63.70 ± 3.50	1.56 ± 0.31
	Everolimus (0.1 μM)	21.95 ± 1.86	1.84 ± 0.28	74.52 ± 4.21	1.69 ± 0.35
	Vinorelbine (1 nM)	44.68 ± 5.11	2.20 ± 0.54	42.59 ± 3.65	10.53 ± 1.14
	Everolimus (0.1 μM) + Vinorelbine (1 nM)	48.38 ± 4.23	1.54 ± 0.28	32.40 ± 1.89	17.68 ± 1.26
HCC25–0705A	Vehicle (control)	28.48 ± 1.89	11.90 ± 1.34	57.71 ± 3.68	1.91 ± 0.30
	Everolimus (0.1 μM)	18.41 ± 1.22	3.0 ± 0.23	66.53 ± 4.29	12.06 ± 1.06
	Vinorelbine (1 nM)	37.23 ± 2.80	5.16 ± 0.34	43.98 ± 2.57	13.63 ± 1.88
	Everolimus (0.1 μM) + Vinorelbine (1 nM)	38.12 ± 2.53	5.94 ± 0.21	41.35 ± 2.64	14.59 ± 2.43

Co-administration of everolimus with vinorelbine augmented tumor growth suppression, diminished cell proliferation markers and positive cell-cycle regulators, and prolonged the lifespan of HCC-engrafted mice

To better elucidate the molecular circuitry through which vinorelbine, when combined with mTOR inhibitors, exerts its antitumor effects, we performed an extensive immunoblotting survey. The protein expression signatures captured from HCC25–0705A tumors harvested after dosing with vinorelbine, everolimus, or everolimus/vinorelbine are depicted in **Figure 3**. Relative to vehicle-exposed controls, vinorelbine monotherapy produced a broad elevation across a panel of proteins: p-p70S6K (Thr389), p-p70S6K (Thr421/Ser424), p-4EBP1 (Thr70), p-Cdc2 (Tyr15), p-Cdk2 (Thr14/Tyr15), p-Rb (Ser807/811), Cyclin B1, p27, survivin, together with the apoptosis-associated cleaved caspase 3 and cleaved caspase 7 fragments. A diametrically opposite expression

pattern emerged in the everolimus monotherapy group, where pronounced depletion was noted for p-mTOR (Ser2448), p-p70S6K (Thr421/Ser424), p-Cdc2 (Tyr15), p-Cdk2 (Thr14/Tyr15), p-Rb (Ser807/811), total Rb protein, Cyclin B1, Cyclin D1, Cdc25, p-Cdc25C (Ser216), and survivin. Everolimus additionally upregulated both p-AKT (Ser473) and p27, while causing p-4EBP1 (Thr70) and p-S6R (Ser235/236) signals to fall below the assay's detectable range when judged against the vehicle lane. The most instructive findings, however, came from the combination arm: everolimus completely negated the vinorelbine-dependent induction of p-p70S6K (at both Thr389 and Thr421/Ser424), p-4EBP1 (Thr70), p-S6R (Ser235/236), p-Cdc2 (Tyr15), p-Cdk2 (Thr14/Tyr15), Cdc25C, p-Rb (Ser807/811), total Rb, Cyclin B1, and survivin. Simultaneously, the dual regimen fostered a robust accumulation of p-AKT (Ser473), p27, cleaved caspase 3, and cleaved caspase 7. A trend toward lower abundance of p-ERK1/2 and Cyclin D1 was also evident in the everolimus/vinorelbine cohort compared with the monotherapy groups.

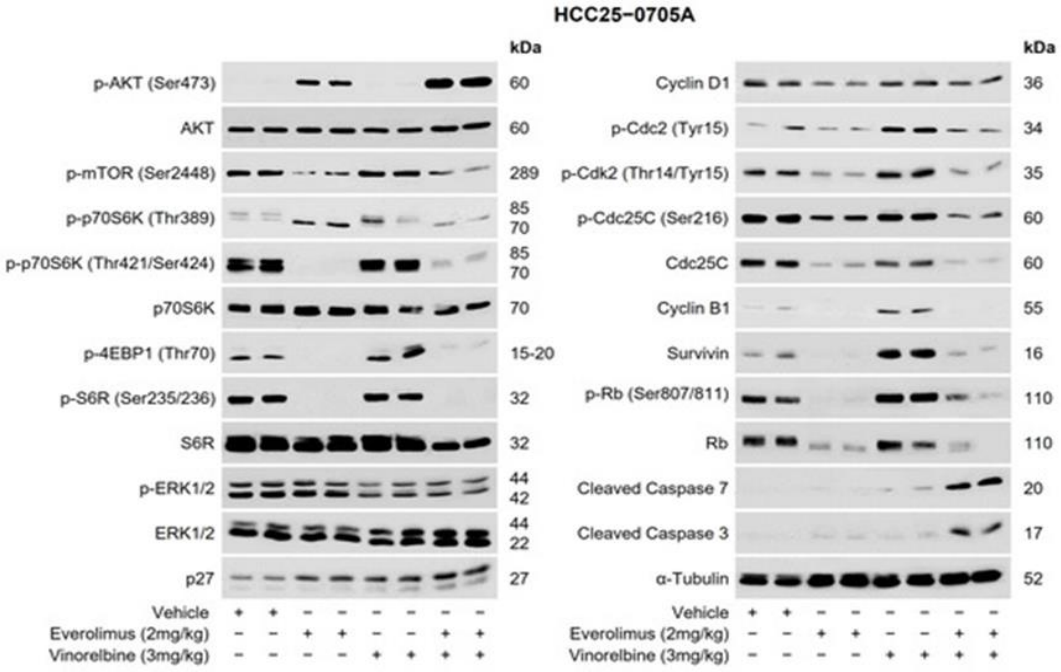

Figure 3. Modulation of the AKT/p70S6K/4EBP1 signaling axis, ERK1/2, and cell-cycle regulatory proteins by everolimus, vinorelbine, and everolimus/vinorelbine. HCC25–0705A tumor fragments were engrafted subcutaneously into SCID mice in accordance with the protocols outlined in Section 4. Once tumors were established, the animals were randomized into four cohorts and dosed orally with 200 µL of vehicle solution, everolimus at 2 mg/kg delivered once per day, vinorelbine at 3 mg/kg injected twice weekly (every 3.5 days), or the combination of everolimus at 2 mg/kg plus vinorelbine at 3 mg/kg over the designated timeframe. Each treatment arm contained 8-10 individually tumor-bearing mice. Tumor specimens were excised at a 2-hour interval after the final dose and processed for immunoblotting as detailed in Section 4. Displayed are representative western blot images probed with the specified primary antibodies, accompanied by the corresponding molecular weight markers (in kDa) for each protein detected.

Seeking to confirm and extend these molecular findings, we performed additional Western blot surveys targeting the identical protein panel across a broader set of HCC PDX lines. The results highlighted model-dependent divergence in the biochemical responses triggered by everolimus, vinorelbine, and the everolimus/vinorelbine doublet. Crucially, the co-delivery of everolimus alongside vinorelbine nullified the vinorelbine-elicited accumulation of p-mTOR (Ser2448), p-p70S6K (both Thr421/Ser424 and Thr389), p-Cdc2 (Tyr15), p-Cdk2 (Thr14/Tyr15), and survivin. At the same time, the combination reinforced the everolimus-characteristic elevation of p-AKT (Ser437) and cleaved caspase 7, while extinguishing detectable expression of both Cdc25 and Cdc2. A modest attenuation of p-ERK1/2 and total Rb was also apparent in tumors from the everolimus/vinorelbine arm. Parallel western blot signatures emerged from the HCC19–0913 PDX model subjected to the same everolimus/vinorelbine protocol, and indistinguishable biochemical outcomes were obtained upon substituting sirolimus for everolimus.

As illustrated in **Figure 4**, Kaplan–Meier survival curves constructed from the three orthotopic HCC models revealed that the entire vehicle-dosed population reached a humane endpoint at 48 days (HCC13–0212), 58 days (HCC24–0309), and 52 days (HCC25–0705A). Single-

modality everolimus and vinorelbine each imparted a statistically significant lifespan extension over vehicle ($P < 0.01$; log-rank test). In the HCC13–0212 orthotopic system, vinorelbine monotherapy outperformed everolimus monotherapy in terms of survival duration (92 versus 74 days). The opposite pattern prevailed in the HCC24–0309 and HCC25–0705A orthotopic settings, where everolimus-treated mice surpassed their vinorelbine-treated counterparts (102 versus 66 days and 106 versus 78 days, respectively). This inversion implies that survival gains from the two single-agent regimens depend on the specific orthotopic model under evaluation. Direct statistical comparison of the everolimus and vinorelbine monotherapy arms confirmed significant inter-group survival differences ($P < 0.05$; log-rank test). The most striking survival advantage, however, was consistently observed in the everolimus/vinorelbine cohorts, which outlived every other treatment group. Median survival in the combination arm reached 130, 150, and 136 days for the HCC13–0212, HCC24–0309, and HCC25–0705A orthotopic models, respectively ($P < 0.01$; log-rank test). These findings firmly establish the superiority of everolimus/vinorelbine over either monotherapy in prolonging OS among mice bearing orthotopically engrafted HCC tumors.

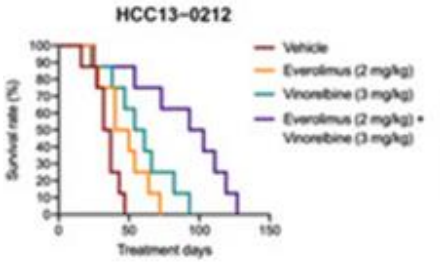

a)

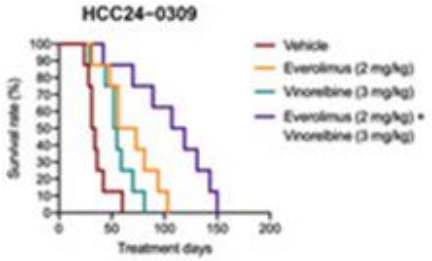

b)

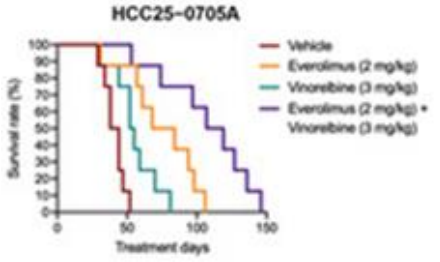

c)

Figure 4. Impact of everolimus, vinorelbine, and the everolimus/vinorelbine combination on the lifespan of animals bearing HCC13–0212, HCC24–0309, and HCC25–0705A orthotopic tumors. Intrahepatic HCC lesions were generated using the surgical technique described in a prior report [30]. Once tumors were established, mice were assigned to receive everolimus alone, vinorelbine alone, or everolimus/vinorelbine over the specified duration, with all dosing parameters executed as outlined in Section 4. Ten mice constituted each treatment arm. Drug administration was initiated after the neoplastic masses reached an estimated volume between 100 and 150 mm^3. Kaplan–Meier survival plots are depicted. The everolimus/vinorelbine doublet conferred a statistically significant prolongation of OS ($P < 0.01$; log-rank test).

Globally, HCC stands as the second most frequent cause of death attributable to cancer [1]. Because a substantial subset of HCC patients are identified at a late, surgically incurable stage, the demand for more effective systemic therapies remains unfulfilled. Although sorafenib [5, 7] and lenvatinib [6] have delivered important progress on this front, the formulation of alternative systemic approaches is indispensable for individuals who either stop responding to or cannot tolerate sorafenib or lenvatinib.

Evidence has emerged that mTOR signaling contributes to tumor-cell insensitivity to microtubule-disrupting drugs and that everolimus administration efficiently counteracts this mTOR-dependent resistance [38]. We reasoned that simultaneously targeting mTOR with an inhibitor and microtubules with a destabilizing agent in HCC might achieve outcomes superior to those of single-drug treatments. To put this premise to the test, we explored the tumor-suppressive capacity of mTOR-blocking compounds (everolimus and sirolimus) together with vinorelbine (a well-characterized microtubule-destabilizing drug) across a panel of HCC PDX models. An additional objective was to refine our understanding of the molecular mechanisms underlying the anticancer properties of vinorelbine, both alone and in combination with everolimus or sirolimus. We describe here the consequences of vinorelbine, everolimus, and the pairings everolimus/vinorelbine or sirolimus/vinorelbine on neoplastic growth, tumor angioarchitecture, cell multiplication, and apoptotic death in 15 HCC PDX models. Administered at 3 mg/kg twice weekly, vinorelbine produced a T/C ratio below 0.42 in 4 of the 15 (26.7%) HCC PDX models evaluated (namely, HCC13–0212, HCC19–0509, HCC13–0109, and HCC19–0913), fulfilling the threshold established by the Cancer Therapy Evaluation Program (CTEP) of the Investigational Drug Branch (IDB) at the National Cancer Institute [34], which denotes that vinorelbine exerted meaningful activity in these four models. Vinorelbine triggered mitotic blockade and apoptotic cell elimination, normalized the tumor

vascular bed, and reduced tumor hypoxia—effects that manifested solely in PDX models responsive to vinorelbine. Western blot analyses indicated that vinorelbine re-engaged the p70S6K/4EBP1 cascade and increased expression of survivin and other cell-cycle regulators in tumors exposed to the drug.

mTOR inhibition delivered as a single modality using everolimus or sirolimus effectively silenced downstream mTOR targets and survivin, translating into tumor growth suppression in 7 of the 15 (46.7%) HCC PDX models (HCC05–0411B, HCC06–1009, HCC13–0212, HCC19–0509, HCC24–0309, HCC25–0705A, and HCC26–0808B). Both mTOR inhibitors promoted normalization of tumor blood vessels, thereby reducing tumor hypoxia. These events were predominantly detected in mTOR-responsive HCC PDX models and were absent from mTOR-unresponsive models, such as HCC29–0909A, HCC09–0913, HCC30–0805B, and HCC29–1104. Within the 15 PDX HCC models subjected to testing, baseline overexpression of p-p706K (Thr421/Ser424) was noted in HCC25–0705A **(Figure 3)**, and HCC05–0411B carried a mutated tuberous sclerosis complex 2 (TSC2) gene [39]. Consistent with predictions, everolimus and sirolimus monotherapies markedly blunted mTOR pathway signaling and diminished the protein levels of survivin and positive cell-cycle regulators, among them p-Cdc2 (Tyr15), p-Cdk2 (Thr14/Tyr15), p-Rb (Ser807/811), Cyclin B1, Cyclin D1, Cdc25, and p-Cdc25C (Ser216), in the HCC25–0705A model. Published reports have proposed that TSC2 status may influence mTOR pathway activity, as TSC2 governs AKT/p70S6K/4EBP1 signaling [39]. Thus, TSC2 loss-of-function, whether through mutation or heightened signaling along the mTOR axis, feeds into the activation of the p70S6K/4EBP1 cascade, which partly explains the sensitivity of the HCC05–0411B and HCC25–0705A PDX models to mTOR inhibitors [39, 40]. Earlier studies across other tumor types [40, 41] and our own findings [39] suggest that mTOR inhibition tends to produce cytostatic arrest rather than complete tumor-cell clearance, suggesting the potential value of combining mTOR blockade with cytotoxic compounds. When conceiving a rational combination regimen, the choice of vinorelbine paired with everolimus was guided by recent evidence demonstrating that vinorelbine-induced microtubule disruption exerts activity against HCC [21, 27-29], alongside the established use of vinorelbine in several other cancer indications [23-26].

The sprouting of new blood vessels is a vital facet of endothelial cell locomotion and tumor evolution. Two approaches to counteract vascular formation involve suppressing angiogenesis and disrupting the integrity of existing tumor vessels using vascular-disrupting compounds [42]. Although vinca alkaloids have been shown to damage the tumor vasculature in animal models [43], our data revealed that vinorelbine treatment increased intratumoral vessel density and promoted vascular normalization, specifically in vinorelbine-sensitive HCC PDX models. Relative to the vasculature observed in vehicle-dosed tumors, the vessels in vinorelbine-treated tumors appeared morphologically thinner in vinorelbine-sensitive PDX models (HCC19–0913, HCC13–0109, HCC13–0212, HCC25–0705A, and HCC24–0309) **(Figure 2)**, whereas no discernible alterations were detected in vinorelbine-resistant PDX models (HCC29–0909A, HCC09–0913, HCC30–0805B, and HCC29–1104). These patterns suggest that vinorelbine induces tumor vascular remodeling events that are selective for and shaped by each model's inherent sensitivity to the drug.

The elevation in intratumoral vessel density following vinorelbine exposure may be explained by the influx of bone-marrow-derived cells (BMDCs) drawn in from neighboring stromal compartments. The accumulation of BMDCs within neoplastic tissue has been shown to promote new vessel growth and aid in the restoration of vascular networks [44, 45]. Even though the pro-angiogenic influence of recruited BMDCs has been linked to tumor shielding and disease relapse [45, 46], the vinorelbine-associated increases in vessel density and normalization coincide with apoptosis and antimitotic effects. Whether the antitumor efficacy exerted by vinorelbine derives from canonical antimitotic interference with microtubule dynamics remains an open question.

The molecular underpinnings of everolimus-mediated blood-vessel normalization remain to be precisely defined. We noted that while the angiogenic vessels embedded within vehicle-treated tumors were excessively enlarged, disorganized, and dysfunctional, the great majority of vessels in tumors responsive to mTOR inhibition were slender, stretched, uniformly structured, and entirely competent, as judged by lectin perfusion assays. It remains to be determined whether the blockade of mTOR downstream targets by everolimus results in reduced vascular endothelial growth factor output and the ensuing normalization of the vasculature. The reduced hypoxia observed in these treated tumors suggests that the compact, capillary-like vessel network re-establishes local oxygen supply. These occurrences seem to hinge on the magnitude of tumor responsiveness to everolimus, since they were not detected in tumors showing comparatively weak sensitivity to either vinorelbine or everolimus.

The everolimus/vinorelbine dual regimen continually produced the most beneficial results, extending to the HCC01–0708, HCC09–0913, HCC05–0614, HCC27–1014, and HCC29–0909A PDX models **(Table 1)**, each of which exhibited relatively low responsiveness to both everolimus and vinorelbine (with a T/C ratio surpassing

0.42). In contrast to the vehicle and single-treatment cohorts, the everolimus/vinorelbine groups showed a pronounced reduction in tumor mass. Earlier publications have indicated that FXYD-domain-containing ion-transport regulator 5 (FXYD5) enhances the insensitivity of HCC cells to sorafenib by stimulating the AKT/mTOR signaling axis [47]. Separately, LINC01234-mediated downregulation of argininosuccinate synthase 1 (ASS1) expression leads to aspartate accumulation and triggers the mammalian target of rapamycin (mTOR) cascade [48]. It is plausible that the increased mTOR signaling observed in the vinorelbine-only arm originated from either raised FXYD5 or diminished ASS1 expression. Hence, inhibiting the mTOR pathway by combining everolimus with vinorelbine can decelerate tumor growth and resensitize HCC tumors that are otherwise refractory to vinorelbine.

Mechanistic explorations revealed that the powerful antitumor impact of everolimus/vinorelbine was matched by decreased levels of p-p70S6K, p-4EBP1, p-S6K, and survivin, each of which was heightened in the vinorelbine-alone group. This result was further supported by elevated rates of mitotic arrest and apoptosis **(Table 3)**. The current body of work indicates that everolimus, when paired with vinorelbine, did not meaningfully modify vinorelbine- or everolimus-induced vascular normalization, ultimately lowering tumor hypoxia **(Figure 2)**. The everolimus/vinorelbine pairing substantially extended OS in mice with orthotopic HCC tumors without causing significant adverse effects, as gauged by body weight, undisturbed food and water consumption, normal social engagement, and animal activity patterns. Mild liver toxicity was noted, reflected by modest elevations in serum markers associated with the vinorelbine and everolimus/vinorelbine dosing **(Table 2)**. Our observations establish that the strong anticancer activity of this dual-inhibitory strategy was partly mediated by vascular normalization and the suppression of proteins that drive survival and cell proliferation. Indeed, contemporary in vivo and in vitro studies have documented that combining the mTOR inhibitor temsirolimus with low-dose vinblastine results in substantial antitumor activity [46]. Prior reports also indicated that this same combination led to a significant decrease in tumor microvessel density relative to vehicle controls, suggesting possible anti-angiogenic activity [49, 50]. By contrast, we detected no notable alterations in microvessel density, lectin perfusion, or tumor hypoxia when vinorelbine-sensitive or everolimus-sensitive tumors were challenged with either the everolimus/vinorelbine or sirolimus/vinorelbine pairing. The divergence between our results and those reported by Zhou *et al*. [49] might be attributable to the distinct mechanisms of action of the two inhibitors (patupilone as a stabilizer versus vinorelbine as a destabilizer) and to the differing HCC model systems used in the two investigations. We assessed the effects of the microtubule-stabilizing drug vinorelbine in HCC PDX models. In contrast, Zhou *et al*. [49] examined the effects of the microtubule-stabilizing agent patupilone in a Hep3B cell xenograft model.

Vascular normalization within tumors has been reported to optimize the delivery of chemotherapeutic drugs in mouse systems, curtail tumor progression, and prolong survival [51-53]. The work presented here demonstrates that vinorelbine or everolimus alone fosters tumor-vessel normalization, and integrating everolimus (or sirolimus) with vinorelbine substantially amplifies the antitumor potency of each agent while extending the OS of mice bearing orthotopic HCC tumors. Our mechanistic assessments have revealed that, in comparison with the antitumor effect exerted by everolimus alone, the striking antitumor efficacy of the combined regimen was not driven by an additional dampening of mTOR pathway activity. These data align closely with a prior report documenting that the temsirolimus–vinblastine combination vigorously suppresses HCC tumor xenograft growth by reducing p70S6K and survivin expression [46]. Moreover, the sirolimus/vinblastine combination [54] and a liposomal preparation co-encapsulating everolimus and vinorelbine [55] exhibited activity against the proliferation of human neuroblastoma and renal cell carcinoma, respectively. Our work and that of others are of considerable importance, particularly in light of the modest single-agent performance of mTOR inhibitors (everolimus and sirolimus) already established in HCC [39-41], set against the documented efficacy of vinorelbine across other cancer indications [27-29, 34, 49, 55]. Further research is needed to more completely map the interactions between everolimus (or sirolimus) and vinorelbine in shaping the tumor response and to clarify the mechanistic basis for their antitumor activity and vessel-normalizing properties. The cooperative growth suppression achieved with everolimus/vinorelbine may be partly explained by vascular normalization, which facilitates drug access to neoplastic cells and subsequently leads to downregulation of mTOR pathway constituents, survivin, and cell-cycle regulatory proteins, along with a heightened apoptotic response.

To mitigate the toxicity inherent to multi-agent regimens, the amount of each drug within the combination often must be scaled back [56]. Employing HCC PDX models and clinically modeled dosing schedules, we offer proof of an intensified tumor response paired with mild hepatic toxicity when vinorelbine is layered onto everolimus. In animal-based investigations, everolimus is conventionally delivered daily by oral gavage at doses spanning 1–5 mg/kg/day [57]. In parallel, vinorelbine is generally administered at a weekly dose of 4.8–5 mg/kg by

intravenous or intraperitoneal injection [58, 59]. In the clinical arena, the adverse events most commonly associated with everolimus include nausea, appetite loss, diarrhea, oral inflammation, pneumonitis, and cutaneous rash [17, 60]. The characteristic toxicities accompanying standard-dose vinorelbine involve neutropenia, peripheral neuropathy, and gastrointestinal (GI) disturbances [37, 61]. A prior endeavor to lessen the side effects attributable to everolimus/vinorelbine gave rise to a tumor-targeted liposomal construct that employs a nominal everolimus dose (1 mg/kg; thrice weekly) together with a lowered vinorelbine dose (0.475 mg/kg; thrice weekly) [55]. This liposomal vehicle co-encapsulating everolimus and vinorelbine drove pronounced tumor control in RCC tumor xenograft models while causing negligible systemic toxicity [55]. Such a liposomal formulation could constitute an encouraging strategy for tackling HCC, a malignancy for which a genuine scarcity of potent therapies persists.

Everolimus and sirolimus exhibit strong immunosuppressive activity and are widely used to dampen immune responses [60]. They disrupt the mTOR signaling hub, which is centrally involved in malignant cell growth, multiplication, new vessel formation, survival, and the fine-tuning between effector T lymphocytes and regulatory T cells (Tregs). Among patients with metastatic renal cell carcinoma, everolimus therapy induced immunological perturbations in circulating immune cell compartments, characterized by expansions of Tregs and monocytic myeloid-derived suppressor cells, and contractions of immunoregulatory natural killer cells, classical CD141+ (cDC1), and CD1c+ (cDC2) dendritic cell subsets [62]. The immunosuppressive effects of everolimus and sirolimus narrow their therapeutic windows in cancer. Future explorations will be required to evaluate whether a low-dose everolimus or sirolimus backbone, partnered with a metronomic vinorelbine schedule or a liposomal preparation co-harboring everolimus and vinorelbine [55], can lessen immune suppression and potentiate T-cell-mediated immunity while preserving antitumor performance.

Conclusion

In sum, using clinically meaningful PDX HCC models and treatment protocols, our investigation reveals that combining mTOR inhibitors (everolimus and sirolimus) with vinorelbine elicits a striking tumor response. Of note, p70S6K/4EBP1 and survivin are extensively overexpressed across the HCC landscape (~70% of cases). Their abundance is closely associated with histological grading of HCC (e.g., high survivin expression serves as an independent prognostic marker of poor outcome in HCC patients) [40, 63]; accordingly, this exceptionally active everolimus/vinorelbine regimen could be particularly significant in routine HCC care as a justified therapeutic choice. The clinical relevance of these findings is further magnified by the economic feasibility of repurposing two long-established, low-cost, and easily deliverable agents (vinorelbine and, particularly, sirolimus), thus ensuring that treatment stays within reach and financially viable for patients. Viewed as a whole, the present body of work provides a robust rationale for the forthcoming phase I/II clinical studies designed to enhance the potency of first-line treatment for individuals diagnosed with HCC.

Acknowledgments: None

Conflict of interest: None

Financial support: This research was supported by the Singapore Ministry of Health's National Medical Research Council under its Ministry of Health Industry Alignment Fund Category 2 (NMRC/MOHIAFCAT2/006/2016), National University Hospital of Singapore Central Grant (CG21APR1005), National University Hospital of Singapore Central Grant (CGAug16M005), National Research Foundation of Singapore under its Competitive Research Program (NRF-CRP17-2017-05), and SingHealth DUKE-NUS Academic Medicine Research Grant (AM/TP049/2021).

Ethics statement: This study received ethics board approval from the SingHealth Centralised Institutional Review Board (ethics code: CIRB #2006/435/B; approval date: 2 October 2018). All the animal procedures were performed according to protocols approved by the SingHealth Institutional Animal Care and Use Committee (IACUC 2014/SHS/904, 2017/SHS/1277, and 2018/SHS/1401).

All the authors have read and agreed to the published version of the manuscript.

References

1. Siegel RL, Miller KD, Jemal A. Cancer statistics, 2017. CA Cancer J Clin. 2017;67(1):7–30.
2. Ferlay J, Soerjomataram I, Dikshit R, Eser S, Mathers C, Rebelo M, et al. Cancer incidence and mortality worldwide: sources, methods and major patterns in GLOBOCAN 2012. Int J Cancer. 2015;136(5):E359–86.
3. Desert R, Nieto N, Musso O. Dimensions of hepatocellular carcinoma phenotypic diversity. World J Gastroenterol. 2018;24(40):4536–47.
4. European Association for the Study of the Liver; European Organization for Research and Treatment of Cancer. EASL-EORTC clinical practice

guidelines: management of hepatocellular carcinoma. J Hepatol. 2012;56(4):908–43.
5. Llovet JM, Ricci S, Mazzaferro V, Hilgard P, Gane E, Blanc JF, et al. Sorafenib in advanced hepatocellular carcinoma. N Engl J Med. 2008;359(4):378–90.
6. Kudo M, Finn RS, Qin S, Han KH, Ikeda K, Piscaglia F, et al. Lenvatinib versus sorafenib in first-line treatment of patients with unresectable hepatocellular carcinoma: a randomized phase 3 non-inferiority trial. Lancet. 2018;391(10126):1163–73.
7. Cheng AL, Kang YK, Chen Z, Tsao CJ, Qin S, Kim JS, et al. Efficacy and safety of sorafenib in patients in the Asia-Pacific region with advanced hepatocellular carcinoma: a phase III randomized, double-blind, placebo-controlled trial. Lancet Oncol. 2009;10(1):25–34.
8. Cheng AL, Qin S, Ikeda M, Galle PR, Ducreux M, Kim TY, et al. Updated efficacy and safety data from IMbrave150: atezolizumab plus bevacizumab vs sorafenib for unresectable hepatocellular carcinoma. J Hepatol. 2022;76(5):862–73.
9. Singal AG, Llovet JM, Yarchoan M, Mehta N, Heimbach JK, Dawson LA, et al. AASLD practice guidance on prevention, diagnosis, and treatment of hepatocellular carcinoma. Hepatology. 2023;78(6):1922–65.
10. Torrens L, Montironi C, Puigvehí M, Mesropian A, Leslie J, Haber PK, et al. Immunomodulatory effects of lenvatinib plus anti-programmed cell death protein 1 in mice and rationale for patient enrichment in hepatocellular carcinoma. Hepatology. 2021;74(6):2652–69.
11. Bruix J, Qin S, Merle P, Granito A, Huang YH, Bodoky G, et al. Regorafenib for patients with hepatocellular carcinoma who progressed on sorafenib treatment (RESORCE): a randomized, double-blind, placebo-controlled, phase 3 trial. Lancet. 2017;389(10064):56–66.
12. Abou-Alfa GK, Meyer T, Cheng AL, El-Khoueiry AB, Rimassa L, Ryoo BY, et al. Cabozantinib (C) versus placebo (P) in patients (pts) with advanced hepatocellular carcinoma (HCC) who have received prior sorafenib: results from the randomized phase III CELESTIAL trial. J Clin Oncol. 2018;36(4 suppl):207.
13. Sangro B, Sarobe P, Hervás-Stubbs S, Melero I. Advances in immunotherapy for hepatocellular carcinoma. Nat Rev Gastroenterol Hepatol. 2021;18(8):525–43.
14. Sahin F, Kannangai R, Adegbola O, Wang J, Su G, Torbenson M. mTOR and P70 S6 kinase expression in primary liver neoplasms. Clin Cancer Res. 2004;10(23):8421–5.
15. Zhou L, Huang Y, Li J, Wang Z. The mTOR pathway is associated with the poor prognosis of human hepatocellular carcinoma. Med Oncol. 2010;27(1):255–61.
16. Buitrago-Molina LE, Pothiraju D, Lamlé J, Marhenke S, Kossatz U, Breuhahn K, et al. Rapamycin delays tumor development in murine livers by inhibiting proliferation of hepatocytes with DNA damage. Hepatology. 2009;50(2):500–9.
17. Zhu AX, Kudo M, Assenat E, Cattan S, Kang YK, Lim HY, et al. EVOLVE-1: phase 3 study of everolimus for advanced HCC that progressed during or after sorafenib. J Clin Oncol. 2014;32(3 suppl):172.
18. Mabuchi S, Altomare DA, Connolly DC, Klein-Szanto A, Litwin S, Hoelzle MK, et al. RAD001 (everolimus) delays tumor onset and progression in a transgenic mouse model of ovarian cancer. Cancer Res. 2007;67(6):2408–13.
19. Patil MA, Chua MS, Pan KH, Lin R, Lih CJ, Cheung ST, et al. An integrated data analysis approach to characterize genes highly expressed in hepatocellular carcinoma. Oncogene. 2005;24(24):3737–47.
20. Tung CY, Jen CH, Hsu MT, Wang HW, Lin CH. A novel regulatory event-based gene set analysis method for exploring global functional changes in heterogeneous genomic data sets. BMC Genomics. 2009;10:26.
21. Zhou Q, Ching AK, Leung WK, Szeto CY, Ho SM, Chan PK, et al. Novel therapeutic potential in targeting microtubules by nanoparticle albumin-bound paclitaxel in hepatocellular carcinoma. Int J Oncol. 2011;38(3):721–31.
22. Higa GM. The microtubule as a breast cancer target. Breast Cancer. 2011;18(2):103–19.
23. Edelstein MP, Wolfe LA, Duch DS. Potentiation of radiation therapy by vinorelbine in non-small cell lung cancer. Semin Oncol. 1996;23(5 Suppl):41–7.
24. Fukuoka K, Arioka H, Iwamoto Y, Fukumoto H, Kurokawa H, Ishida T, et al. Mechanism of the radiosensitization induced by vinorelbine in human non-small cell lung cancer cells. Lung Cancer. 2001;34(3):451–60.
25. Krzakowski M, Lucas C, Gridelli C. Fractionated scheme of oral vinorelbine as single-agent therapy or in combination with cisplatin concomitantly with thoracic radiotherapy in stage III non-small-cell lung cancer: dose-escalation phase I trial. Clin Lung Cancer. 2014;15(4):266–73.
26. Strøm HH, Bremnes RM, Sundstrøm SH, Helbekkmo N, Aasebø U. Poor prognosis patients with inoperable locally advanced NSCLC and large tumors benefit from palliative chemoradiotherapy: a subset analysis

from a randomized clinical phase III trial. J Thorac Oncol. 2014;9(6):825–33.
27. Huynh H, Lee LY, Goh KY, Ong R, Hao HX, Huang A, et al. Infigratinib mediates vascular normalization, impairs metastasis, and improves chemotherapy in hepatocellular carcinoma. Hepatology. 2019;69(3):943–58.
28. Huynh H, Prawira A, Le TBU, Vu TC, Hao HX, Huang A, et al. FGF401 and vinorelbine synergistically mediate antitumor activity and vascular normalization in FGF19-dependent hepatocellular carcinoma. Exp Mol Med. 2020;52(11):1857–68.
29. Yeoh KW, Prawira A, Saad MZB, Lee KM, Lee EMH, Low GK, et al. Vinorelbine augments radiotherapy in hepatocellular carcinoma. Cancers (Basel). 2020;12:872. 34
30. Huynh H, Koong HN, Poon D, Choo SP, Toh HC, Thng CH, et al. AZD6244 enhances the anti-tumor activity of sorafenib in ectopic and orthotopic models of human hepatocellular carcinoma. J Hepatol. 2010;52(1):79–87. 60-62
31. National Research Council (US), Institute for Laboratory Animal Research (US). Guide for the care and use of laboratory animals. Washington (DC): National Academies Press; 2011.
32. Yang Y, Zhu J, Gou H, Cao D, Jiang M, Hou M. Clinical significance of Cox-2, survivin and Bcl-2 expression in hepatocellular carcinoma. Med Oncol. 2011;28(3):796–803.
33. Huynh H, Soo KC, Chow PK, Panasci L, Tran E. Xenografts of human hepatocellular carcinoma: a useful model for testing drugs. Clin Cancer Res. 2006;12(6):4306–14. 30-33
34. Cancer Therapy Evaluation Program (CTEP)—Investigational Drug Branch (IDB). National Cancer Institute. Available from: https://ctep.cancer.gov/branches/idb/default.htm [cited 2023 Dec 9].
35. Gabardi S, Baroletti SA. Everolimus: a proliferation signal inhibitor with clinical applications in organ transplantation, oncology, and cardiology. Pharmacotherapy. 2010;30(10):1044–56.
36. Motzer RJ, Escudier B, Oudard S, Hutson TE, Porta C, Bracarda S, et al. Phase 3 trial of everolimus for metastatic renal cell carcinoma: final results and analysis of prognostic factors. Cancer. 2010;116(17):4256–65.
37. Xu YC, Wang HX, Tang L, Ma Y, Zhang FC. A systematic review of vinorelbine for the treatment of breast cancer. Breast J. 2013;19(2):180–8. 35
38. VanderWeele DJ, Zhou R, Rudin CM. Akt up-regulation increases resistance to microtubule-directed chemotherapeutic agents through mammalian target of rapamycin. Mol Cancer Ther. 2004;3(12):1605–13.
39. Huynh H, Hao HX, Chan SL, Chen D, Ong R, Soo KC, et al. Loss of tuberous sclerosis complex 2 (TSC2) is frequent in hepatocellular carcinoma and predicts response to mTORC1 inhibitor everolimus. Mol Cancer Ther. 2015;14(5):1224–35.
40. Tam KH, Yang ZF, Lau CK, Lam CT, Pang RW, Poon RT. Inhibition of mTOR enhances chemosensitivity in hepatocellular carcinoma. Cancer Lett. 2009;273(2):201–9.
41. Wang L, Shi WY, Wu ZY, Varna M, Wang AH, Zhou L, et al. Cytostatic and anti-angiogenic effects of temsirolimus in refractory mantle cell lymphoma. J Hematol Oncol. 2010;3:30.
42. Tozer GM, Kanthou C, Baguley BC. Disrupting tumour blood vessels. Nat Rev Cancer. 2005;5(5):423–35.
43. Dumontet C, Jordan MA. Microtubule-binding agents: a dynamic field of cancer therapeutics. Nat Rev Drug Discov. 2010;9(10):790–803.
44. Du R, Lu KV, Petritsch C, Liu P, Ganss R, Passegué E, et al. HIF1α induces the recruitment of bone marrow-derived vascular modulatory cells to regulate tumor angiogenesis and invasion. Cancer Cell. 2008;13(3):206–20.
45. Murdoch C, Muthana M, Coffelt SB, Lewis CE. The role of myeloid cells in the promotion of tumour angiogenesis. Nat Rev Cancer. 2008;8(10):618–31.
46. Zhou Q, Lui VW, Lau CP, Cheng SH, Ng MH, Cai Y, et al. Sustained antitumor activity by co-targeting mTOR and the microtubule with temsirolimus/vinblastine combination in hepatocellular carcinoma. Biochem Pharmacol. 2012;83(6):1146–58.
47. Tan XP, Xiong BH, Zhang YX, Wang SL, Zuo Q, Li J. FXYD5 promotes sorafenib resistance through the Akt/mTOR signaling pathway in hepatocellular carcinoma. Eur J Pharmacol. 2022;931(6):175186.
48. Chen M, Zhang C, Liu W, Du X, Liu X, Xing B. Long noncoding RNA LINC01234 promotes hepatocellular carcinoma progression through orchestrating aspartate metabolic reprogramming. Mol Ther. 2022;30(9):2354–69.
49. Zhou Q, Wong CH, Lau CP, Hui CW, Lui VW, Chan SL, et al. Enhanced antitumor activity with combining effect of mTOR inhibition and microtubule stabilization in hepatocellular carcinoma. Int J Hepatol. 2013;2013:103830.
50. Campostrini N, Marimpietri D, Totolo A, Mancone C, Fimia GM, Ponzoni M, et al. Proteomic analysis of anti-angiogenic effects by a combined treatment with vinblastine and rapamycin in an endothelial cell line. Proteomics. 2006;6(19):4420–31.

51. Park JS, Kim IK, Han S, Park I, Kim C, Bae J, et al. Normalization of tumor vessels by Tie2 activation and Ang2 inhibition enhances drug delivery and produces a favorable tumor microenvironment. Cancer Cell. 2016;30(5):953–67.
52. Mpekris F, Baish JW, Stylianopoulos T, Jain RK. Role of vascular normalization in benefit from metronomic chemotherapy. Proc Natl Acad Sci U S A. 2017;114(6):1994–9.
53. Cantelmo AR, Conradi LC, Brajic A, Goveia J, Kalucka J, Pircher A, et al. Inhibition of the glycolytic activator PFKFB3 in endothelium induces tumor vessel normalization, impairs metastasis, and improves chemotherapy. Cancer Cell. 2016;30(50):968–85.
54. Marimpietri D, Brignole C, Nico B, Pastorino F, Pezzolo A, Piccardi F, et al. Combined therapeutic effects of vinblastine and rapamycin on human neuroblastoma growth, apoptosis, and angiogenesis. Clin Cancer Res. 2007;13(15):3977–88.
55. Pal K, Madamsetty VS, Dutta SK, Mukhopadhyay D. Co-delivery of everolimus and vinorelbine via a tumor-targeted liposomal formulation inhibits tumor growth and metastasis in RCC. Int J Nanomedicine. 2019;14:5109–23.
56. Lopez JS, Banerji U. Combine and conquer: challenges for targeted therapy combinations in early phase trials. Nat Rev Clin Oncol. 2017;14(1):57–66.
57. O'Reilly T, McSheehy PM, Wartmann M, Lassota P, Brandt R, Lane HA. Evaluation of the mTOR inhibitor everolimus in combination with cytotoxic antitumor agents using human tumor models in vitro and in vivo. Anticancer Drugs. 2011;22(1):58–78.
58. Sinha S, Cao Y, Dutta S, Wang E, Mukhopadhyay D. VEGF neutralizing antibody increases the therapeutic efficacy of vinorelbine for renal cell carcinoma. J Cell Mol Med. 2010;14(3-4):647–58.
59. Tsuruo T, Inaba M, Tashiro T, Yamori T, Ohnishi Y, Ashizawa T, et al. Evaluation of antitumor activity of navelbine against human breast carcinoma xenografts. Anticancer Drugs. 1994;5(5):634–40.
60. Houghton PJ. Everolimus. Clin Cancer Res. 2010;16(4):1368–72.
61. Gregory RK, Smith IE. Vinorelbine—a clinical review. Br J Cancer. 2000;82(10):1907–13.
62. Huijts CM, Santegoets SJ, de Jong TD, Verheul HM, de Gruijl TD, van der Vliet HJ. Immunological effects of everolimus in patients with metastatic renal cell cancer. Int J Immunopathol Pharmacol. 2017;30(3-4):341–52.
63. Huynh H, Ngo VC, Koong HN, Poon D, Choo SP, Thng CH, et al. Sorafenib and rapamycin induce growth suppression in mouse models of hepatocellular carcinoma. J Cell Mol Med. 2009;13(8):2673–83.